RBSC-NVSS SAMPLE. I. RADIO AND OPTICAL IDENTIFICATIONS OF A COMPLETE SAMPLE OF 1500 BRIGHT X-RAY SOURCES

Franz E. Bauer[1]

National Radio Astronomy Observatory[2]
Department of Astronomy, University of Virginia,
520 Edgemont Road, Charlottesville, VA 22903
E-mail: fbauer@nrao.edu

J. J. Condon

National Radio Astronomy Observatory[2]
520 Edgemont Road, Charlottesville, VA 22903
E-mail: jcondon@nrao.edu

Trinh X. Thuan

Department of Astronomy, University of Virginia,
P.O. Box 3818, Charlottesville, VA 22903-3818
E-mail: txt@virginia.edu

and

J. J. Broderick

Department of Physics, Virginia Polytechnic Institute and State University
Blacksburg, Virginia 24061
E-mail: jjb@vt.edu

ABSTRACT

We cross-identified the *ROSAT* Bright Source Catalog (RBSC) and the NRAO VLA Sky Survey (NVSS) to construct the RBSC-NVSS sample of the brightest X-ray sources (≥ 0.1 counts s^{-1} $\sim 10^{-12}$ ergs cm^{-2} s^{-1} in the 0.1–2.4 keV band) that are also radio sources ($S \geq 2.5$ mJy at 1.4 GHz) in the 7.8 sr of extragalactic sky with $|b| > 15°$ and $\delta > -40°$. The sky density of NVSS sources is low enough that they can be reliably identified with RBSC sources having rms positional uncertainties $\geq 10''$. We used

[1]Visiting Astronomer, Kitt Peak National Optical Observatories, operated by the Association of Universities for Research in Astronomy, Inc., under contract with the National Science Foundation

[2]The National Radio Astronomy Observatory is a facility of the National Science Foundation operated under cooperative agreement by Associated Universities, Inc.

the more accurate radio positions to make reliable X-ray/radio/optical identifications down to the POSS plate limits. We obtained optical spectra for many of the bright identifications lacking published redshifts. The resulting X-ray/radio sample is unique in its size ($N \sim 1500$ objects), composition (a mixture of nearly normal galaxies, Seyfert galaxies, quasars, and clusters), and low average redshift ($\langle z \rangle \sim 0.1$).

Subject headings: catalogs — radio continuum: general — surveys — X-rays: general

1. INTRODUCTION

The *ROSAT* All-Sky Survey Bright Source Catalogue (Voges et al. 1999, RBSC revision 1RXS) contains the first large all-sky sample of the brightest X-ray sources, analogous in many respects to the optical NGC catalog. It was derived from the soft (0.1–2.4 keV) X-ray survey performed during the first half year of the *ROSAT* mission in 1990/91. The catalog sky coverage is 92%, and there are 8,547 sources above its 0.1 counts s^{-1} ($\sim 10^{-12}$ ergs s^{-1} cm^{-2}) completeness limit. Bade et al. (1998) found that about one third of the RBSC sources can be reliably identified with galactic stars, while most of the rest are extragalactic. The extragalactic content of the RBSC comprises a diverse blend of (1) normal spiral galaxies whose X-ray emission is powered by stars and stellar remnants, (2) elliptical galaxies with hot gaseous halos, (3) AGN in Seyfert galaxies, elliptical galaxies, quasars, and BL Lac objects, and (4) clusters of galaxies. The large number of sources in this catalog easily permits statistical analyses of *each* type of X-ray object. However, the essential properties of these X-ray sources cannot be determined from the X-ray data alone—we need observations in optical and other wavebands to measure their distances, identify their energy sources, etc. Such observations are possible only for those RBSC sources whose optical counterparts have been identified. In this paper we present reliable radio and optical identifications for sources in the RBSC complete sample.

Most RBSC sources have rms positional uncertainties $\geq 10''$ and the sky density of faint optical objects is high, so only the nearest extragalactic X-ray sources can be optically identified by position coincidence alone (cf. Bade et al. 1998). Fortunately, most extragalactic RBSC sources are also radio sources in the 1.4 GHz NRAO/VLA Sky Survey (Condon et al. 1998a, NVSS), whose sky density is low enough for identification with RBSC sources. Since the radio positions are significantly more accurate, the radio sources may be optically identified, yielding optical identifications for the corresponding X-ray sources as well. The NVSS covers the 10.3 sr of sky north of $\delta = -40°$ and contains over 1.8×10^6 sources stronger than its 2.5 mJy beam^{-1} completeness limit. Since the NVSS was made with relatively low resolution ($45''$ FWHM), it does not discriminate against moderately extended radio sources in nearby galaxies and clusters. Its rms positional uncertainties range from $< 1''$ for the $N \approx 4 \times 10^5$ sources stronger than 15 mJy to $7''$ for the faintest (S = 2.3 mJy) detectable sources, allowing us to make optical identifications with objects as faint as R ≈ 21.

We optically identified the RBSC-NVSS sources with objects in the United States Naval Observatory catalog A2.0 (Monet et al. 1998, USNO). The USNO catalog contains 526,280,881 objects detected by the Precision Measuring Machine on the Palomar Optical Sky Survey I (POSS-I) blue O and red E plates, the UK Science Research Council SRC-J survey plates, and the European Southern Observatory ESO-R survey plates. The catalog was compiled from the blue/red overlaps (within $2''$) of the detection lists generated from scans of POSS-I O and E plates centered on $\delta > -18^\circ$ and SRC-J and ESO-R plates centered on $\delta < -20^\circ$. The stated astrometric and photometric errors are about $0\farcs25$ and 0.5 mag rms, respectively. The USNO catalog covers the entire sky and probes as deep as B=21 (O plates), R=20 (E plates), J=22, and F=21 for objects with appropriate colors.

Section 2 explains our method for making the identifications and assessing their reliabilities. The results are presented in Section 3.

2. Cross-identifications

In this section we present a sequence of increasingly powerful methods for making cross-identifications and directly evaluating the their individual reliabilities: (1) The simplest case is identification by position-coincidence between two wavebands (Sec. 2.1), associating NVSS radio sources with RBSC X-ray sources, for example. For each candidate we derive the probability that it is the correct identification (the reliability of that identification). (2) If the positions are not sufficiently accurate to guarantee reliable identifications by themselves, they may be supplemented by additional data (Sec. 2.2). To continue our example, RBSC X-ray sources have a flatter radio flux-density distribution than NVSS background sources, so radio flux densities affect identification reliabilities. The identification reliabilities derived directly in this section are similar to those obtained via the "likelihood ratio" method by Sutherland & Saunders (1992). (3) Even with the aid of additional data, the RBSC position errors are too large for making reliable X-ray identifications with faint optical objects. We show how accurate positions of NVSS radio sources associated with RBSC sources can be used to select the correct optical counterparts. The reliabilities of such multiwavelength linked position-coincidence identifications are derived in (Sec. 2.3). (4) Finally, linked cross-identifications can themselves be strengthened by applying additional constraints (e.g., optical magnitudes), and their reliabilities are obtained in Section 2.4.

2.1. Direct Position-coincidence Identifications

All identification programs begin with a set of identification candidates in some search area surrounding each source to be identified. This area should encompass all plausible candidates, but its exact size and shape are not critical. A larger than necessary search area increases the number of candidates which must be evaluated but does not significantly degrade identification reliability.

We used search circles of $180''$ in radius (Figure 1) to identify RBSC sources having rms positional uncertainties $\sigma_{\rm x} \approx 10'' - 20''$. The search radius is much larger than the 3σ X-ray error circle to permit identification with extended and asymmetric radio sources. Each search area contains some numbers $m \geq 0$ of NVSS radio sources and $l \geq 0$ of optical objects from the USNO catalog.

We consider radio identifications of X-ray sources using only the X-ray and radio positions. Let $P(R)$ $(R = 1, \ldots, m)$ represent the probability that the R^{th} candidate is the correct radio identification of an X-ray source and $P(0)$ the probability that none is. Since there is only a negligible chance that the radio identification is exterior to the search area, $P(0)$ is just the probability that the actual identification is too faint to be recognized as a candidate. For example, we cannot identify radio counterparts fainter than the 2.5 mJy beam^{-1} NVSS catalog limit. Such an identification is often called an "empty field." If we make the *astronomical* assumption that not more than one of the m candidates is the correct identification, then the sum of these mutually exclusive probabilities is unity:

$$\sum_{R=0}^{m} P(R) = 1 \ . \tag{1}$$

The R^{th} candidate is the correct identification if (1) there exists a detectable identification, (2) that identification lies in the infinitesimal area element dA containing the position of the R^{th} candidate, and (3) the $(m-1)$ remaining candidates are unrelated sources which happen to lie in the areas dA surrounding their positions (see Figure 1). The probability that all three independent events occur is the product of their individual probabilities, which we now evaluate.

(1) The *a priori* probability that there is a detectable radio identification is equal to the initially unknown fraction $f_{\rm r}$ of X-ray sources in the sample that actually have detectable radio identifications. We estimated $f_{\rm r}$ by guessing an initial value, making trial identifications for the whole source sample, replacing the initial value by the observed value, and iterating. If this procedure fails to converge rapidly, the resulting identifications are probably too unreliable to be useful. To estimate the observed value of $f_{\rm r}$ we summed the computed reliabilities of all the RBSC-NVSS identifications and divided that sum by the total number of X-ray sources. Since only a small percentage of bright galactic X-ray stars are radio sources, we calculated separate $f_{\rm r}$ values for fields containing optically bright $(m < 12)$ stars and for all other fields.

(2) The probability of finding the correct identification in the infinitesimal area dA offset by the angle $\phi_{\rm xr}(R)$ between the position of the X-ray source and the R^{th} candidate is $p[\phi_{\rm xr}(R)]dA$, where $p[\phi_{\rm xr}(R)]$ is just the normalized error distribution of the measured X-ray/radio offsets. These errors include both the radio and X-ray measurement errors and may be augmented by a contribution allowing for possible astronomical offsets of extended sources. For example, the centroid of a head-tail radio source will not coincide with its parent galaxy.

(3) If the R^{th} candidate is the correct identification, then the remaining $(m-1)$ candidates must be unrelated sources lying in areas dA containing their positions. The probability of finding each unrelated source is $\rho_{\rm r} dA$, where $\rho_{\rm r}$ is the mean sky density of unrelated radio candidates. For

NVSS candidates,

$$\rho_{\rm r} = \int_{S_{\rm min}}^{\infty} n(S) dS \ , \tag{2}$$

where $n(S)$ is the differential source count at 1.4 GHz and $S_{\rm min} = 2.5$ mJy is the minimum flux density of the candidates. Possible clustering of candidates around the true identification could be addressed by increasing $\rho_{\rm r}$ from its global to local value. If there is no detectable identification, all m candidates must be unrelated sources.

The resulting set of $(m+1)$ proportionalities

$$P(R) \propto f_{\rm r} p[\phi_{\rm xr}(R)] dA (\rho_{\rm r} dA)^{m-1} \qquad \text{if } R > 0 \tag{3a}$$

$$P(0) \propto (1 - f_{\rm r})(\rho_{\rm r} dA)^m \tag{3b}$$

normalized by Equation 1 specify the $(m+1)$ identification reliabilities:

$$P(R) = c f_{\rm r} \frac{p[\phi_{\rm xr}(R)]}{\rho_{\rm r}} \qquad \text{if } R > 0 \tag{4a}$$

$$P(0) = c(1 - f_{\rm r}) \ , \tag{4b}$$

where

$$c^{-1} = \frac{f_{\rm r}}{\rho_{\rm r}} \sum_{j=1}^{m} p[\phi_{\rm xr}(j)] + (1 - f_{\rm r}) \ . \tag{4c}$$

Equation 4 gives the probability $P(R)$ that the R^{th} of m candidates is the correct identification and the probability $P(0)$ that none is. These probabilities depend on the search area only through the number m of candidates contributing to the sum in Equation 4c. Making the search area "too big" by definition only adds candidates having negligible $p(\phi_{\rm xr})$ and hence little effect in Equation 4c.

In many cases, the positional error distributions of both the source and its identification candidates are nearly circular Gaussians. [See Condon et al. (1995) for the more complicated case of elliptical Gaussian error distributions with arbitrary orientations.] If the X-ray source and radio candidate positions have rms uncertainties $\sigma_{\rm x}$ and $\sigma_{\rm r}$ in each coordinate, then

$$p(\phi_{\rm xr}) = \frac{1}{2\pi\sigma^2} \exp\left(-\frac{\phi_{\rm xr}^2}{2\sigma^2} \right) \ , \tag{5}$$

where $\sigma^2 \equiv \sigma_{\rm x}^2 + \sigma_{\rm r}^2$. The variance of $\phi_{\rm xr}$ is $\langle \phi_{\rm xr}^2 \rangle = 2\sigma^2$ so a typical identification has $p(\phi_{\rm xr}) \sim (2\pi\sigma^2 e)^{-1}$ and is highly reliable if both

$$\sigma^2 \ll \frac{f_{\rm r}}{2\pi e \rho_{\rm r}(1 - f_{\rm r})} \tag{6a}$$

and

$$\sigma^2 \ll \frac{1}{2\pi e \rho_{\rm r}} \tag{6b}$$

Equation 6a ensures that true empty fields are not misidentified with background sources, a danger if the actual identification rate is very low ($f_{\rm r} \ll 1$). Equation 6b ensures that there is no difficulty choosing the correct identification from multiple candidates. For NVSS identifications of extragalactic RBSC sources, $f_{\rm r} \approx 0.61$ and the sky density of sources stronger than the NVSS catalog limit $S_{\rm min} \approx 2.5$ mJy is $\rho_{\rm r} \approx 1.76 \times 10^5$ sr^{-1}, leading to the fairly weak requirement $\sigma \ll 10^2$ arcsec which is easily satisfied by the RBSC positional uncertainties. The sky density of optical objects in the USNO catalog is two orders of magnitude higher, and the RBSC positional uncertainties are too large to satisfy the requirement $\sigma \ll 10$ arcsec for making optical identifications by position coincidence alone, even though most RBSC sources do have optical counterparts in the USNO catalog.

2.2. Pairwise Identifications With Additional Constraints

Uncertain identifications based on positional coincidence alone may be strengthened or rejected by non-positional data. For example, the flux-density distribution of radio sources identified with extragalactic RBSC sources peaks well above the NVSS sensitivity limit. Figure 2 shows the logarithm of the ratio of the probability $p[S|x]$ that a RBSC-NVSS source has flux density S to the probability $p[S|\overline{x}]$ that an unrelated NVSS sources has flux density S. Most unrelated radio sources are fainter than the correct identifications (indicated in Figure 2 by the positive logarithm of the ratio at all but the faintest radio flux levels), so the stronger of two radio candidates with similar $p(\phi_{\rm xr})$ is the more likely identification. The reliabilities of such identifications can be calculated through the use of "likelihood ratios" (see Sutherland & Saunders 1992); here we obtain the identification reliabilities directly by extending the derivation of Equation 4.

Let $p[\phi_{\rm xr}(R), S(R)]dAdS$ be the probability that the R^{th} candidate is the identification lying in the area dA surrounding its observed position and in the flux-density range dS containing its observed flux density $S(R)$. The multiplicative law of probabilities states that this probability is the product of $p[\phi_{\rm xr}(R)]dA$ and $p[S(R)|x]dS$, where $p(S|x)$ is the normalized ($\int_{S_{\rm min}}^{\infty} p(S|x)dS = 1$) flux-density distribution of radio sources identified with X-ray sources. Like $f_{\rm r}$, $p(S|x)$ is best estimated from the actual identification data by iteration. The probability that the R^{th} candidate is an unrelated (X-ray quiet) radio source with flux density S lying in area dA is $p[S(R)|\overline{x}]\rho_{\rm r} dAdS$, where $p(S|\overline{x})$ is the flux-density distribution of all (background) NVSS sources. Thus Equations 3 and 4 can be replaced by:

$$P(R) \propto f_{\rm r} p[\phi_{\rm xr}(R)] \frac{p[S(R)|x]}{p[S(R)|\overline{x}]} dAdS \left\{ \prod_{j=1}^{m} p[S(j)|\overline{x}] \right\} (\rho_{\rm r} dAdS)^{m-1} \qquad \text{if } R > 0 \tag{7a}$$

$$P(0) \propto (1 - f_{\rm r})\left\{\prod_{j=1}^{m} p[S(j)]|\overline{x}]\right\}(\rho_{\rm r} dA dS)^m \tag{7b}$$

and

$$P(R) = c f_{\rm r} \frac{p[\phi_{\rm xr}(R)]}{\rho_{\rm r}} \frac{p[S(R)|x]}{p[S(R)|\overline{x}]} \qquad \text{if } R > 0 \tag{8a}$$

$$P(0) = c(1 - f_{\rm r}) \tag{8b}$$

where

$$c^{-1} = \frac{f_{\rm r}}{\rho_{\rm r}} \sum_{j=1}^{m} p[\phi_{\rm xr}(j)] \frac{p[S(j)|x]}{p[S(j)|\overline{x}]} + (1 - f_{\rm r}) \tag{8c}$$

Equation 8 gives the identification probabilities based on candidate flux densities as well as positional coincidence. It could be further extended to include additional continuous (e.g., spectral index) or discrete (e.g., morphological type) parameters which might prove useful for distinguishing between correct identifications and unrelated candidates.

2.3. Linked Position-coincidence Cross-identifications

The positional uncertainties of most RBSC sources are too large to yield reliable optical identifications with faint galaxies and quasars directly. However, the NVSS sources reliably identified with RBSC sources have sufficiently accurate radio positions that nearly all can be optically identified by position coincidence alone. The reliabilities of such linked X-ray/radio/optical position-coincidence identifications are derived below.

Let $P(R, V)$ be the probability that the R^{th} radio source and the V^{th} optically visible object are the correct identifications of an X-ray source, where $R = 0, 1, \ldots, m$ and $V = 0, 1, \ldots, l$. The values $R = 0$ and $V = 0$ correspond to radio and optical "empty fields," respectively. The probabilities of these $(m+1)(l+1)$ mutually exclusive possible outcomes must add up to one:

$$\sum_{R=0}^{m} \sum_{V=0}^{l} P(R, V) = 1 \ . \tag{9}$$

Denote the fractions of X-ray sources in the sample having detectable ($R > 0$) radio and optical ($V > 0$) identifications by f_r and f_v, respectively. Let $p[\phi_{\rm xr}(R)]$ and $p[(\phi_{\rm xv}(V)]$ be the probability densities of the X-ray/radio and X-ray/optical positional offsets ϕ if the R^{th} radio source and the V^{th} optical object are the correct identifications. The sky densities of background radio and optical candidates are $\rho_{\rm r}$ and $\rho_{\rm v}$, respectively. Using the multiplication law $P(R, V) = P(R)P(V|R)$ yields:

$$P(R, V) \propto f_{\rm r} p[\phi_{\rm xr}(R)] dA (\rho_{\rm r} dA)^{m-1} f_{\rm v} p[\phi_{\rm xv}(V)] dA (\rho_{\rm v} dA)^{l-1} \qquad \text{if } R > 0, V > 0 \tag{10a}$$

$$P(R,0) \propto f_{\rm r} p[\phi_{\rm xr}(R)] dA (\rho_{\rm r} dA)^{m-1} (1-f_{\rm v})(\rho_{\rm v} dA)^{l} \qquad \text{if } R>0 \tag{10b}$$

$$P(0,V) \propto (1-f_{\rm r})(\rho_{\rm r} dA)^{m} f_{\rm v} p[\phi_{\rm xv}(V)] dA (\rho_{\rm v} dA)^{l-1} \qquad \text{if } V>0 \tag{10c}$$

$$P(0,0) \propto (1-f_{\rm r})(\rho_{\rm r} dA)^{m} (1-f_{\rm v})(\rho_{\rm v} dA)^{l} \tag{10d}$$

The normalization Equation 9 then implies:

$$P(R,V) = c f_{\rm r} f_{\rm v} \frac{p[\phi_{\rm xr}(R)]}{\rho_{\rm r}} \frac{p[\phi_{\rm xv}(V)]}{\rho_{\rm v}} \qquad \text{if } R>0, V>0 \tag{11a}$$

$$P(R,0) = c f_{\rm r} (1-f_{\rm v}) \frac{p[\phi_{\rm xr}(R)]}{\rho_{\rm r}} \qquad \text{if } R>0 \tag{11b}$$

$$P(0,V) = c (1-f_{\rm r}) f_{\rm v} \frac{p[\phi_{\rm xv}(V)]}{\rho_{\rm v}} \qquad \text{if } V>0 \tag{11c}$$

$$P(0,0) = c(1-f_{\rm r})(1-f_{\rm v}) \ , \tag{11d}$$

where

$$c^{-1} = \frac{f_{\rm r} f_{\rm v}}{\rho_{\rm r}\rho_{\rm v}} \sum_{j=1}^{m} p[\phi_{\rm xr}(j)] \sum_{i=1}^{l} p[\phi_{\rm xv}(i)]$$

$$+ \frac{f_{\rm r}(1-f_{\rm v})}{\rho_{\rm r}} \sum_{j=1}^{m} p[\phi_{\rm xr}(j)] + \frac{(1-f_{\rm r}) f_{\rm v}}{\rho_{\rm v}} \sum_{i=1}^{l} p[\phi_{\rm xv}(i)] + (1-f_{\rm r})(1-f_{\rm v}) \ . \tag{11e}$$

Unfortunately, applying Equation 11 does not yield good optical identifications of RBSC X-ray sources because both the X-ray positional uncertainties and the mean density $\rho_{\rm v}$ of optical candidates are large. Reliable radio identifications of X-ray sources can be made because the density $\rho_{\rm r}$ of radio candidates is much smaller, and reliable optical identifications of NVSS radio sources are possible because the NVSS positions are more accurate. If the *astronomical* assumption is made that the optical identifications of these radio identifications are also the optical identifications of the corresponding X-ray sources, then

$$P(R,V) \propto f_{\rm r} p[\phi_{\rm xr}(R)] dA (\rho_{\rm r} dA)^{m-1} f_{\rm v} p[\phi_{\rm xv}(V)] dA (\rho_{\rm v} dA)^{l-1} p[\phi_{\rm rv}(R,V)] dA (\rho_{\rm v} dA)^{l-1}$$

$$\text{if } R>0, V>0 \tag{12a}$$

$$P(R,0) \propto f_{\rm r} p[\phi_{\rm xr}(R)] dA (\rho_{\rm r} dA)^{m-1} (1-f_{\rm v})(\rho_{\rm v} dA)^l (\rho_{\rm v} dA)^l \qquad \text{if } R > 0 \tag{12b}$$

$$P(0,V) \propto (1-f_{\rm r})(\rho_{\rm r} dA)^m f_{\rm v} p[\phi_{\rm xv}(V)] dA (\rho_{\rm v} dA)^{l-1} (\rho_{\rm v} dA)^l \qquad \text{if } V > 0 \tag{12c}$$

$$P(0,0) \propto (1-f_{\rm r})(\rho_{\rm r} dA)^m (1-f_{\rm v})(\rho_{\rm v} dA)^l (\rho_{\rm v} dA)^l \ , \tag{12d}$$

where $p[\phi_{\rm rv}(R,V)]$ is the probability distribution of offsets between the R^{th} radio source and the V^{th} optical object. The normalization Equation 9 implies

$$P(R,V) = c f_{\rm r} f_{\rm v} \frac{p[\phi_{\rm xr}(R)]}{\rho_{\rm r}} \frac{p[\phi_{\rm xv}(V)]}{\rho_{\rm v}} \frac{p[\phi_{\rm rv}(R,V)]}{\rho_{\rm v}} \qquad \text{if } R > 0, V > 0 \tag{13a}$$

$$P(R,0) = c f_{\rm r} (1-f_{\rm v}) \frac{p[\phi_{\rm xr}(R)]}{\rho_{\rm r}} \qquad \text{if } R > 0 \tag{13b}$$

$$P(0,V) = c (1-f_{\rm r}) f_{\rm v} \frac{p[\phi_{\rm xv}(V)]}{\rho_{\rm v}} \qquad \text{if } V > 0 \tag{13c}$$

$$P(0,0) = c(1-f_{\rm r})(1-f_{\rm v}) \ , \tag{13d}$$

where

$$c^{-1} = \frac{f_{\rm r} f_{\rm v}}{\rho_{\rm r} \rho_{\rm v}^2} \sum_{j=1}^{m} p[\phi_{\rm xr}(j)] \sum_{i=1}^{l} p[\phi_{\rm xv}(i)] p[\phi_{\rm rv}(j,i)]$$

$$+ \frac{f_{\rm r}(1-f_{\rm v})}{\rho_{\rm r}} \sum_{j=1}^{m} p[\phi_{\rm xr}(j)] + \frac{(1-f_{\rm r}) f_{\rm v}}{\rho_{\rm v}} \sum_{i=1}^{l} p[\phi_{\rm xv}(i)] + (1-f_{\rm r})(1-f_{\rm v}) \ . \tag{13e}$$

Equation 13 specifies the reliabilities of linked X-ray/radio/optical identifications made on the basis of position-coincidence alone.

2.4. Linked Cross-identifications With Additional Constraints

Finally, differences between the magnitude distributions of the optical counterparts to X-ray sources and background optical objects can be used to improve the reliability of the optical identifications. Figure 3 gives the logarithm of the ratio of the probability $p[\mu|x]$ that the USNO identification of a RBSC-NVSS source has magnitude μ to the probability $p[\mu|\overline{x}]$ that an unrelated USNO object has magnitude μ as a function of B magnitude, and shows, in contrast to the radio, that there is very little difference between the two populations for B > 13, but the ratio does become large for objects brighter than this limit. Let $\mu(V)$ denote the magnitude of the V^{th}

optical candidate. Let $p(\mu|x)$ and $p(\mu|\overline{x})$ be the normalized magnitude distributions of optical objects in the USNO catalog which are X-ray sources and unrelated optical objects, respectively. Let $p(S|x)$ be the normalized flux-density distribution of radio-detected X-ray sources and $p(S|\overline{x})$ be the the normalized flux-density distribution of unrelated radio sources stronger than the NVSS limit, 2.5 mJy. Then

$$P(R,V) \propto f_{\rm r} p[\phi_{\rm xr}(R)] \frac{p[S(R)|x]}{p[S(R)|\overline{x}]} dAdS \left\{ \prod_{j=1}^{m} p[S(j)|\overline{x}] \right\} (\rho_{\rm r} dAdS)^{m-1}$$

$$\times f_{\rm v} p[\phi_{\rm xv}(V)] \frac{p[\mu(V)|x]}{p[\mu(V)|\overline{x}]} dAd\mu \left\{ \prod_{i=1}^{l} p[\mu(i)|\overline{x}] \right\} (\rho_{\rm v} dAd\mu)^{l-1}$$

$$\times p[\phi_{\rm rv}(R,V)] dA (\rho_{\rm v} dA)^{l-1} \qquad \text{if } R > 0, V > 0 \tag{14a}$$

$$P(R,0) \propto f_{\rm r} p[\phi_{\rm xr}(R)] \frac{p[S(R)|x]}{p[S(R)|\overline{x}]} dAdS \left\{ \prod_{j=1}^{m} p[S(j)|\overline{x}] \right\} (\rho_{\rm r} dAdS)^{m-1}$$

$$\times (1 - f_{\rm v}) \left\{ \prod_{i=1}^{l} p[\mu(i)|\overline{x}] \right\} (\rho_{\rm v} dAd\mu)^{l} (\rho_{\rm v} dA)^{l} \qquad \text{if } R > 0 \tag{14b}$$

$$P(0,V) \propto (1 - f_{\rm r}) \left\{ \prod_{j=1}^{m} p[S(j)|\overline{x}] \right\} (\rho_{\rm r} dAdS)^{m}$$

$$\times f_{\rm v} p[\phi_{\rm xv}(V)] \frac{p[\mu(V)|x]}{p[\mu(V)|\overline{x}]} dAd\mu \left\{ \prod_{i=1}^{l} p[\mu(i)|\overline{x}] \right\} (\rho_{\rm v} dAd\mu)^{l-1} (\rho_{\rm v} dA)^{l} \qquad \text{if } V > 0 \tag{14c}$$

$$P(0,0) \propto (1 - f_{\rm r}) \left\{ \prod_{j=1}^{m} p[S(j)|\overline{x}] \right\} (\rho_{\rm r} dAdS)^{m}$$

$$\times (1 - f_{\rm v}) \left\{ \prod_{i=1}^{l} p[\mu(i)|\overline{x}] \right\} (\rho_{\rm v} dAd\mu)^{l} (\rho_{\rm v} dA)^{l} \ . \tag{14d}$$

The normalized probabilities are:

$$P(R,V) = c f_{\rm r} f_{\rm v} \frac{p[\phi_{\rm xr}(R)]}{\rho_{\rm r}} \frac{p[S(R)|x]}{p[S(R)|\overline{x}]} \frac{p[\phi_{\rm xv}(V)]}{\rho_{\rm v}} \frac{p[\mu(V)|x]}{p[\mu(V)|\overline{x}]} \frac{p[\phi_{\rm rv}(R,V)]}{\rho_{\rm v}}$$

$$\text{if } R > 0, V > 0 \tag{15a}$$

$$P(R,0) = cf_{\rm r}(1-f_{\rm v})\frac{p[\phi_{\rm xr}(R)]}{\rho_{\rm r}}\frac{p[S(R)|x]}{p[S(R)|\overline{x}]} \qquad \text{if } R > 0 \tag{15b}$$

$$P(0,V) = c(1-f_{\rm r})f_{\rm v}\frac{p[\phi_{\rm xv}(V)]}{\rho_{\rm v}}\frac{p[\mu(V)|x]}{p[\mu(V)|\overline{x}]} \qquad \text{if } V > 0 \tag{15c}$$

$$P(0,0) = c(1-f_{\rm r})(1-f_{\rm v})\ , \tag{15d}$$

where

$$c^{-1} = f_{\rm r}f_{\rm v}\sum_{j=1}^{m}\frac{p[\phi_{\rm xr}(j)]}{\rho_{\rm r}}\frac{p[S(j)|x]}{p[S(j)|\overline{x}]}\sum_{i=1}^{l}\frac{p[\phi_{\rm xv}(i)]}{\rho_{\rm v}}\frac{p[\mu(i)|x]}{p[\mu(i)|\overline{x}]}\frac{p[\phi_{\rm rv}(j,i)]}{\rho_{\rm v}}$$

$$+f_{\rm r}(1-f_{\rm v})\sum_{j=1}^{m}\frac{p[\phi_{\rm xr}(j)]}{\rho_{\rm r}}\frac{p[S(j)|x]}{p[S(j)|\overline{x}]} + (1-f_{\rm r})f_{\rm v}\sum_{i=1}^{l}\frac{p[\phi_{\rm xv}(i)]}{\rho_{\rm v}}\frac{p[\mu(i)|x]}{p[\mu(i)|\overline{x}]}$$

$$+(1-f_{\rm r})(1-f_{\rm v})\ . \tag{15e}$$

It is with Equation 15 that we evaluated the reliabilities of the RBSC identification candidates found in Section 3.

The final identification process proceeded as follows. We started with a list of X-ray positions and errors from the RBSC. We then searched for corresponding NVSS radio and USNO optical sources within a $3'$ radius ($R = 0, \ldots, m$ and $V = 0, \ldots, l$ respectively). This particular search size was used because it was much larger than the 3σ X-ray error circle and large enough to contain all but the most extended radio and optical sources. The positions of these sources (X-ray, radio, and optical), their positional errors, and their fluxes and magnitudes were combined with the *a priori* probabilities of detecting radio and optical counterparts, $f_{\rm r}$ and $f_{\rm v}$, the RBSC radio flux and optical magnitude distributions using Equation 15 to estimate the probabilities, $P(R,V)$. We estimated $f_{\rm r}$ and $f_{\rm v}$ initially , and then iteratively replaced these values with the actual identification rates until they converged to the values of 0.61 and 0.99. The RBSC flux and magnitude distributions were again found iteratively. The radio flux distribution of RBSC sources was compared to the distribution of background NVSS objects and the RBSC optical magnitude distribution was compared to the position dependent optical background distribution given by Bahcall & Soneira (1980).

2.5. Additional Parameters and Possible Concerns

Many astronomical objects have extended X-ray, radio, or optical structures which lead to offsets between wavebands beyond those accounted for by measurement errors.

To allow for an offset between the centroid and central component of a radio source smaller than the NVSS beam, we added one tenth of the deconvolved NVSS size or upper limit in quadrature to the rms uncertainty of the NVSS centroid position. Further, if this RBSC-NVSS matched field happened to lie within the area covered by the VLA FIRST Survey (White et al. 1997, $5''$ resolution, 1 mJy flux limit), we then evaluated Equation 15, and replaced the NVSS sources with the FIRST sources if the reliability was better.

An attempt was also made to identify sources resolved into two or more NVSS components, such as double-lobed or head-tail radio galaxies. If two radio components in the search area were within $3'$ of one another and had a flux ratio < 3, we initiated a test for a double source. This consisted of adding an artificial "source" with the combined flux of the two components and located at their radio centroid (this gave much better results than the *optimally* weighted centroid used in Windhorst et al. 1984) to the candidate list. We then re-evaluated Equation 15, keeping this new "source" if the reliability was greater than 0.8 or reverting back to the original reliability estimation otherwise. The rms major- and minor-axis position errors for these artificial sources were taken to be $\frac{1}{10}$ and $\frac{1}{30}$ the size of the component separation. We also found a few true double sources with flux ratios > 3 which were evaluated in the same manner.

We have not corrected for extended RBSC sources. This has the effect of selecting against large scale X-ray emission not coincident with optical and radio sources, such as clusters of galaxies.

Since the USNO catalog does not list optical angular sizes, we used the AIPS Gaussian fitting task IMFIT to measure the optical diameters of of objects larger than $0\rlap{.}'5$. An additional error of $\frac{1}{15}$ of the major axis was added in quadrature with the rms optical positional uncertainty (which we took to be $0\rlap{.}''5$).

The USNO O plate magnitudes are converted into Johnson B magnitudes using $B = O - 0.119(O - E)$ (Evans 1988). We found that these USNO magnitudes are systematically too bright for galaxies with B $\lesssim 16$ by as much as three magnitudes in both R and B as shown by a comparison of USNO magnitudes with B magnitudes from the NASA/IPAC Extragalactic Database (NED 1999) (Figure 4). There is better agreement (the dispersion is ~ 2 mag) between USNO and NED magnitudes for galaxies with B $\gtrsim 16$. To avoid overestimating the identification reliabilities of objects brighter than B ≈ 16, we corrected the USNO blue magnitudes using the polynominal fit

$$\mathrm{B_{NED}} = -0.066 + 1.172\mathrm{B_{USNO}} + 0.120(\mathrm{B_{USNO}})^2 - 0.014(\mathrm{B_{USNO}})^3 + 0.000376(\mathrm{B_{USNO}})^4$$

indicated by the solid curve in Figure 4. The remaining scatter ($\pm$ 2 mag) is not large enough to impact the reliability of our identifications since the ratio $p(\mu|x)/p(\mu|\overline{x})$ does not change by more than a factor of a few over the affected magnitude range (Fig. 3).

One problem associated with catalogued flux densities and magnitudes is Malmquist bias. Given some error in the flux and magnitude determination and the steep slope of the counts, the true brightness of an object will be overestimated. While this is a potential pitfall for faint flux and magnitude counts, it should not significantly affect the reliabilities calculated here for several reasons: 1) the flux and magnitude estimates are normalized by the same Malmquist biased background, 2) for the optical sources, the flat magnitude distribution (Fig. 3) carries little weight in the reliability determination anyway, and 3) the slope of the optical (and to a lesser extent the radio) RBSC source counts turns over well in advance of the survey limit, such that there are very few faint sources where the bias would be strongest.

A further complication is the high sky density of bright foreground stars at low Galactic latitudes. The likelihood that an optical star is an X-ray emitter is quite large (one third of RBSC sources are stellar in origin; (Bade et al. 1998)), while the likelihood that the same optical star is also a radio emitter is quite small ($\sim 0.1 - 2\%$, see Condon et al. (1997)). Thus a bright X-ray star near a background radio source may result in the identification of the X-ray star with that radio source. Because the density of background optical sources increases more rapidly toward fainter magnitudes than the density of RBSC-NVSS optical identifications does, a bright optical star will be assigned a greater identification reliability than a faint galaxy, even if the star is not quite as close to the radio position as the galaxy is. Weeding out X-ray objects which are likely to be stars will then decrease the chances of calling an interloper the correct identification. Thus we classified all objects brighter than B $<$ 13 mag on the basis of appearance on the Digitized Sky Survey (Lasker et al. 1990, DSS) as stars (with diffraction spikes, saturated point source, no diffuse halo) or galaxies. X-ray fields containing one or more bright stars but no bright galaxies within 3σ of the X-ray position were considered stellar. In these cases, the value of f_r was forced to be 0.02 for stellar fields rather than 0.61, the extragalactic identification fraction. We may have missed a few radio stars with high proper motions because the USNO2 and radio positions were measured at different epochs.

Finally, we used the locally measured, rather than global, surface density $\rho_{\rm v}$ of background objects because many RBSC sources reside in optically overdense regions (clusters of galaxies).

3. Identification Results

For the parent sample, we selected the 5441 RBSC sources above the 0.1 counts s^{-1} completeness limit with Galactic latitudes $|b| > 15°$ (to reduce the number of objects which might confuse optical identification and minimize extinction at both optical and X-ray wavelengths) and J2000 $\delta > -40°$, the NVSS declination limit. Of these, 1773 sources are readily identified as stars, in agreement with Bade et al. (1998). We attempted to make *linked* X-ray/radio/optical cross-identifications using X-ray/radio and radio/optical positional coincidence supplemented by radio flux densities and optical magnitudes, as described in Section 2.4.

We visually confirmed each match by overlaying the contours of the NVSS image and the RBSC error box on the DSS (see Figure 5). In addition, the IRAS Faint Source Catalogue (Moshir et al. 1992, FSC) has been matched against the RBSC (see Condon et al. 1998b), so we have plotted the FSC 3σ error ellipses to aid identification and differentiate between physical emission processes. The nearest candidate usually has the highest calculated reliability (Equation 15), although the radio emission for some sources is extended and more care had to be taken in locating an optical counterpart. We use the term *association* to describe extended X-ray/radio sources which appear related but may not be spatially coincident. For instance, a cluster of galaxies may contain one or more radio galaxies and hot intercluster X-ray gas. We retained 19 identifications with low calculated reliabilities on the basis of other information, such as detection in a *ROSAT* pointed observation or no obvious optical counterpart within the error circle. All deviations from the standard reliability estimate are noted in Section 3.1. The reliabilities of these sources are given as '–'.

Some RBSC-NVSS sources had no USNO sources listed near their NVSS positions, but objects were clearly visible on the DSS (i.e the red plate). Most were either very bright, extended galaxies or very faint objects. USNO sources were identified based on a positional coincidence of within $2\farcs0$ on the red and blue plates, so we might expect that some bright galaxies will have red and blue emission peaks separated by more than $2\farcs0$ and thus be rejected. For these we used positions and magnitudes from NED. Furthermore, the faint objects we find must only appear on the red plate (the lack of a blue plate counterpart presumably excluded them from the USNO catalog). We used the AIPS task IMFIT to measure their positions. Faint object magnitudes were estimated by comparison with nearby USNO sources.

These additional sources were added to the USNO list of optical candidates located within the search area and evaluated as part of the standard reliability calculation (see Equation 15). This additional step introduces a slight bias in the reliabilities of these new faint sources, because we have only added the faint sources in close proximity to the radio/X-ray positions, and not those from the rest of the $3'$ radius field. We can test the statistical error of this effect by simply doubling the number of local background objects; this is akin to probing roughly 2 magnitudes fainter than the USNO. While the change will depend on the exact field, we found the reliability with this background enhancement typically differed by only 1% (and at most 5%).

The Galactic absorption corrected X-ray fluxes come from the RBSC correlation catalogue (Voges et al. 1999), in which the RBSC count rate was converted to flux assuming a power law photon energy distribution of the form $\mathrm{E}^{-\Gamma_x+1}$, common to AGN and clusters of galaxies. An average photon index $\langle\Gamma_\mathrm{x}\rangle = 2.3$ was used, typical of extragalactic objects (Hasinger, Trümper & Schmidt 1991) over the *ROSAT* energy range. Corrections for Galactic absorption were based on hydrogen column densities $\mathrm{N_H}$ obtained from Dickey & Lockman (1990).

The error of the unabsorbed X-ray flux is about 30% taking into account errors in photon statistics and variable Galactic absorption. Flux estimates break down for cases when the actual

Γ_x deviates significantly from the mean value, there is additional intrinsic absorption, or when a single power law model inadequately describes the spectral shape (see Brinkmann et al. (1995) for a more detailed discussion of this problem).

A total of 1556 RBSC-NVSS sources were identified, on the criterion that the sum total of all radio identification reliabilities be greater than 0.50. The vast majority exceeded this cut-off limit a large margin. The distribution of RBSC-NVSS sources on the sky is fairly uniform (Figure 6). Roughly one half of the extragalactic RBSC sources did not have radio counterparts. Only 1 RBSC-NVSS source has no detectable optical counterpart (not surprising given the large RBSC error circles and the density of optical sources at the limiting magnitude of the POSS). Table 1 lists the 44 possible galactic stars so identified because they have $B < 13$ mag, diffraction spikes, faint irregular radio contours or a spectral type from SIMBAD. Many have been independently verified with high resolution VLA images to be radio stars by Condon et al. (1997). Table 1 is arranged in the following manner:

Column 1. *ROSAT* BSC name, format 1RXS JHHMMSS.S+DDMMSS.
Column 2. SIMBAD Common Name, if available.
Column 3. *ROSAT* RBSC X-ray Flux.
Column 4. NVSS position, unless otherwise noted.
Column 5. NVSS 1.4 GHz Flux density.
Column 6. Identification Probability P(R,V) (Equation 15). Identifications with a '−' have been accepted despite having a low probability.
Column 7. SIMBAD object type, if available. Abbreviations from SIMBAD as follows:

*	=	Star
Al	=	Eclipsing binary of Algol type
bL	=	Eclipsing binary of Beta Lyr type
Cl	=	Star or globular cluster
DQ	=	Cataclysmic variable of DQ Her type
Fl	=	Flare star
Mi	=	Variable star of Mira Cet type
Pu	=	Pulsating variable star
Ro	=	Rotationally variable star
RS	=	Star of RS CVn type
sr	=	Semi-regular pulsating star
TT	=	T Tau-type star
V	=	Variable star
PN	=	Planetary nebula

Column 8. SIMBAD B magnitude, if available; otherwise USNO magnitude enclosed in parentheses.
Column 9. SIMBAD spectral type, if available.

The remaining 1512 objects are extragalactic and listed in Table 2. Figure 7 shows the cumulative fraction of identifications versus reliability. The vast majority ($\sim 70\%$) of identifications have reliabilities greater than 99%. Table 2 is arranged in the following manner:

Column 1. *ROSAT* RBSC name, format 1RXS JHHMMSS.S+DDMMSS.
Column 2. NED Common Name, if available.
Column 3. *ROSAT* BSC X-ray Flux.
Column 4. NVSS position, unless noted otherwise.
Column 5. NVSS 1.4 GHz Flux density.
Column 6. Identification Probability P(R,V) (Equation 15). Identifications with a '−' have been accepted despite having a low probability.
Column 7. B magnitude from NED, if available; otherwise from USNO as indicated by '()'. Identifications with a '−' denote empty fields.
Column 8. Redshift, if known. From NED unless noted otherwise. Identifications with a '−' represent objects for which spectra was taken but a redshift could not be determined. Identifications with a '?' represent objects for which spectra is of poor quality and the redshift determination is questionable. We have obtained optical spectra with the KPNO 2.1 m telescope for many of the bright identifications which did not possess published redshifts. Helio-centric redshifts are given for these objects. The detailed description of these spectra will be given in a subsequent paper (Bauer, Thuan & Condon 2000).
Column 9. NED optical morphology, if available.
Column 10. Spectral classification, if known. From NED unless noted otherwise in redshift column.

AGN	=	Active galactic nuclei, type unknown
Blazar	=	BL Lacertae type object with variable emission line spectra
BLLAC	=	BL Lacertae type object
BLRG	=	Broad-line radio galaxy
cD	=	Central dominant galaxy, Early-type stellar absorption continuum
Early	=	Early-type stellar absorption continuum
HII	=	Starburst galaxy with narrow emission-line spectra similar to HII regions
HPQ	=	High polarization QSO
LINER	=	Low ionization narrow emission-line region
LPQ	=	Low polarization QSO
QSO	=	Quasi-stellar object
Sy1-2	=	Seyfert galaxy, emission-line spectra classified from type 1 to 2

There are a small number of cases having low reliabilities, but which may in fact be true identifications. They generally fall into two categories; objects needing higher radio resolution and candidates that have optical/radio matches farther than 3σ from the X−ray source which did not have a convincing optical match. Many of the latter are likely to be associated with nearby clusters.

3.1. Notes on Individual Identifications

1RXS J000312.3−355541: Member of cluster Abell 2717.
1RXS J001031.3+105832: Member of triple galaxy III Zw 002.
1RXS J001118.5−285126: Member of cluster Abell 2734. Diffuse radio emission; possible radio halo?
1RXS J001823.8+300357: Member of group WP 01.
1RXS J001906.0−202638: Cluster Abell S0026 is 50″ from ID and overlaps within positional errors.
1RXS J002041.8−254307: Member of cluster Abell 0022.
1RXS J002136.8+280305: Group IV Zw 015 is 77″ from ID and overlaps within positional errors.
1RXS J002430.5−292856: Extended radio emission.

1RXS J002534.9−330255: Greater than 3σ from X−ray position. Low X−ray flux and large error region imply unreliable X−ray position. Optical and radio information point towards a correlation. Member of cluster ABELL S0041.
1RXS J002811.6+310342: Possible ID is not at 002812.61+310315.3 (as identified in RGB). Better radio resolution would strengthen ID.
1RXS J003037.6−241053: Member of cluster Abell 0047.
1RXS J003413.7−212619: Member of group SCG 05.
1RXS J004324.9−203728: Probable member of cluster Abell 2813.
1RXS J004924.0−293128: Probable member of cluster Abell S0084.
1RXS J010721.2+322254: Greater than 3σ from X−ray position. Low X−ray flux and large error region imply unreliable X−ray position. Optical and radio information point towards a correlation. Member of group IV Zw 038.
1RXS J010750.4−364342: Member of cluster Abell 2871.
1RXS J010850.5−152438: Member of cluster Abell 0151.
1RXS J011301.1+153041: Member of cluster Abell 0160. Given the low X−ray flux and large error region imply unreliable X−ray position. Optical and radio information point towards a correlation.
1RXS J011354.9−314538: Greater than 3σ from X−ray position. Given the low X−ray flux and large error region imply unreliable X−ray position. Optical and radio information point towards a correlation. Pointed *ASCA* observation by Arimoto et al. 1997 confirms ID. Member of cluster Abell S0141.
1RXS J011513.2+405743: More reliable ID is a blend of star and galaxy on DSS.
1RXS J012058.3−135100: Member of cluster CID 10.
1RXS J012337.2+331506: Member of pair ARP 229.
1RXS J012507.3+084124: Member of cluster Abell 0193.
1RXS J012910.8−214158: Galaxy composed of two compact optical cores.
1RXS J013152.8−133651: Member of cluster Abell 0209.
1RXS J013632.9+390556: KPNO spectrum obtained. No features revealed amid strong blue continuum.
1RXS J013715.1−091145: Member of cluster CID 12.
1RXS J015244.7+360855: Member of cluster Abell 0262.
1RXS J015705.3+412029: Member of cluster Abell 0276.
1RXS J020144.2−021158: Member of cluster Abell 0291.
1RXS J023727.6−263027: Probable member of cluster Abell 0368.
1RXS J024122.1−283919: Cluster Abell 3041 is $53''$ from ID and overlaps within positional errors.
1RXS J024620.0−301639: Supernova SN 1992bd is $1''$ from ID and is also a valid identification.
1RXS J024937.1−311114: Member of cluster Abell S0301.
1RXS J030150.6+355003: Member of group UGC 02489 and cluster Abell 0407. V Zw 311 NOTES02 appears to be a cD from DSS and is likely to be true ID. Better radio resolution needed to clarify.
1RXS J031611.4+090445: KPNO spectrum obtained. No features revealed amid the flat continuum.
1RXS J033828.8−352701: Member of Fornax cluster.
1RXS J041325.4+102756: Probable member of cluster Abell 0478.
1RXS J042551.3−083329: Member of cluster EXO 0422−086.
1RXS J042700.9−204321: Probable member of cluster Abell 0490.
1RXS J043337.7−131528: Member of cluster Abell 0496.
1RXS J043643.8+100323: Member of cluster MS 0433.9+0957.
1RXS J043902.0+052050: Member of cluster RX J04390+0520.
1RXS J044511.8−155118: Member of cluster CID 25.
1RXS J044803.3−202741: High resolution radio position from Owen, White & Ge (1993) confirms ID. Member of cluster Abell 0514.
1RXS J044814.8+095259: Member of cluster RX J0448.2+0952.
1RXS J045859.6−002904: Member of cluster CID 27.
1RXS J050049.4−384038: Member of cluster Abell 3301.
1RXS J050120.1−033223: High resolution radio position from Owen, White & Ge (1993) confirms ID. Member of cluster Abell 0531.
1RXS J050507.9−322007: Probable member of cluster Abell 3313.
1RXS J051611.5−000807: RBSC position incorrect. X-ray observations from Ceballos & Barcons (1996) confirm ID.
1RXS J054738.7−315228: Member of cluster Abell 3364.
1RXS J055040.7−321619: Cluster Abell S0549 ($z = 0.04030$) is $13''$ from ID and overlaps well within positional errors.
1RXS J055711.1−372813: Probable member of cluster Abell S0555.
1RXS J060552.7−351759: Probable member of cluster Abell 3378.
1RXS J062707.5−352917: Member of cluster Abell 3392.
1RXS J064326.5+421420: High resolution radio position from Laurent-Muehleisen et al. (1997) confirms ID.

1RXS J070427.0+631856: Member of cluster Abell 0566.
1RXS J070907.6+483657: Member of cluster Abell 0569.
1RXS J071006.0+500243: High resolution radio position from Laurent-Muehleisen et al. (1997).
1RXS J073221.5+313750: Probable member of cluster Abell 0586.
1RXS J074144.8+741444: Member of cluster ZwCl 0735.7+7421.
1RXS J074238.0+092213: Member of cluster Abell 0592. Better radio resolution needed.
1RXS J081021.3+421657: Member of cluster [VMF98] 047.
1RXS J081112.3+700300: Member of cluster Abell 0621
1RXS J081929.5+704221: Very extended radio and optical emission associated with the dwarf galaxy Holmberg II.
1RXS J082209.5+470601: Member of cluster Abell 0646.
1RXS J083811.0+245336: Member of pair CGCG 120−011.
1RXS J083950.7−121424: High resolution radio position from Li & Jin (1996) confirm ID as [HB89] 0837-120 and not [EYG89] 087.
1RXS J084255.9+292752: Member of cluster ZwCl 0839.9+2937.
1RXS J091037.2+332920: KPNO spectrum obtained. No features revealed among strong blue continuum.
1RXS J091949.1+334532: X-ray position offset, but Einstein observations from Fabbiano, Kim & Trinchieri (1992) confirm ID. Member of cluster Abell 0779.
1RXS J092406.1+141002: Member of cluster Abell 0795.
1RXS J094740.4−305655: Member of triple galaxy AM 0945−304.
1RXS J095821.8−110344: Member of cluster Abell 0907.
1RXS J100121.5+555351: Member of cluster [YGK80] 0957+561CLUSTER. QSO [HB89] 0957+561 and galaxy [YGK81] 097 are $4''$ and $9''$ from ID and overlap within positional errors.
1RXS J100639.1+255450: Member of cluster Abell 0923.
1RXS J101335.9−135108: Member of cluster RX J10136−1350.
1RXS J101912.1+635802: Member of pair CGCG 313−011.
1RXS J102228.9+500630: Member of cluster Abell 0980.
1RXS J102339.3+041117: Member of cluster ZwCl 1021.0+0426.
1RXS J102350.7−271522: Member of cluster Abell 3444.
1RXS J102758.9−064804: Member of cluster RX J1027.9-0648.
1RXS J103155.8−141659: Multiple redshift systems overlap within positional errors.
1RXS J103459.5+304138: Member of cluster Abell 1045.
1RXS J104043.7+395706: Probable member of cluster Abell 1068.
1RXS J104431.7−070404: Member of cluster Abell 1084.
1RXS J104651.9−253546: Member of cluster RX J10468−2535
1RXS J105344.2+492956: Member of cluster MS 1050.7+4946.
1RXS J105825.9+564716: Probable member of cluster Abell 1132.
1RXS J111137.2+405031: Member of cluster Abell 1190.
1RXS J111422.6+582318: High resolution radio position from Laurent-Muehleisen et al. (1997) confirms ID.
1RXS J111450.1−121351: Cluster Abell 1211 is $89''$ from ID and overlaps within positional errors.
1RXS J113121.4+333447: Member of cluster Abell 1290.
1RXS J113153.7−195543: Member of cluster Abell 1300.
1RXS J113222.4+555828: Galaxy MCG +09−19−110 ($z = 0.05130$) is $17''$ from ID and overlaps within positional errors. Member of cluster RX J1132.3+5558.
1RXS J113448.4+490438: Member of cluster Abell 1314.
1RXS J114124.2−121632: Member of cluster RX J1141.4−1216.
1RXS J114442.2+672435: Member of cluster Abell 1366. Optical and radio information point towards a correlation. Possible X-ray cluster emission?
1RXS J114452.7+194706: Greater than 3σ from RBSC position. Public *ROSAT* HRI observations place X−ray source much closer to reliable ID. Association with cluster Abell 1367.
1RXS J114947.0−121845: Probable member of Abell 1391. Association?
1RXS J115518.9+232431: Member of cluster Abell 1413. taken from the FIRST 1.4 GHz survey (White et al. 1997). NVSS flux density is 5.4 mJy. Member of cluster RX J11570+2415.
1RXS J115719.0+333645: High resolution radio position from Owen, White & Ge (1993) confirms more reliable ID. Member of cluster Abell 1423.
1RXS J120511.7+392043: Member of cluster RX J1205.1+3920
1RXS J121105.4+352005: Member of cluster RX J1211.0+3520
1RXS J122752.7+632317: Member of cluster RX J1227.8+6323.
1RXS J122945.9+075927: Member of cluster Virgo S.

1RXS J123658.8+631111: Member of cluster Abell 1576.
1RXS J124349.3−153320: Probable member of cluster Abell 1603.
1RXS J125233.7−311605: Member of cluster RX J12525−3116.
1RXS J125422.2−290034: Member of cluster Abell 3528.
1RXS J125710.0−172345: Pointed *ROSAT* observation from Peres et al. (1998) confirms ID. Member of cluster Abell 1644.
1RXS J125921.5−041131: Member of cluster Abell 1651.
1RXS J130250.3−023041: Probable member of cluster Abell 1663.
1RXS J130343.6−241506: Member of cluster Abell 1664.
1RXS J130346.7+191635: Member of cluster Abell 1668.
1RXS J130552.6+305405: Member of cluster Abell 1677.
1RXS J130916.1−013658: Member of cluster MS 1306.7−0121.
1RXS J131129.5−012017: Member of cluster Abell 1689.
1RXS J131506.8+514931: Member of cluster Abell 1703.
1RXS J132016.3+330828: Member of cluster RX J1320.1+3308.
1RXS J132542.1−022800: No optical counterpart on DSS.
1RXS J132549.2+591937: Member of cluster Abell 1744.
1RXS J132617.4+001329: Member of cluster RX J1326.3+0013.
1RXS J132758.9−313027: Greater than 3σ from RBSC position. Optical and radio information point towards a correlation. Member of cluster Abell 3558. Possible X-ray blend of star and galaxy?
1RXS J133226.0−330812: Better radio resolution confirms ID.
1RXS J134104.8+395942: Probable member of cluster Abell 1774.
1RXS J134152.6+262230: Cluster Abell 1775 ($z = 0.06960$) is $72''$ from ID and overlaps within positional errors.
1RXS J134730.5−114455: Member of cluster RX J13475−1145.
1RXS J134852.6+263541: Member of cluster Abell 1795.
1RXS J140102.1+025249: Member of cluster Abell 1835.
1RXS J140337.0−335840: Member of cluster Abell S0753.
1RXS J140728.4−270055: Member of cluster Abell 3581.
1RXS J141342.6+433938: Member of cluster Abell 1885.
1RXS J141357.3+711751: Probable association with cluster Abell 1895 ($z = 0.22492$).
1RXS J142139.7+371743: Member of cluster Abell 1902.
1RXS J143236.0+313855: Cluster Abell 1930 ($z = 0.13130$) is $119''$ from ID and overlaps within positional errors.
1RXS J143527.9+550747: Member of cluster Abell 1940.
1RXS J144428.4+311304: Cluster Abell 1961 ($z = 0.23200$) is $117''$ from ID and overlaps within positional errors.
1RXS J145307.8+215333: Probable member of cluster Abell 1986.
1RXS J145431.4+183834: Member of cluster Abell 1991.
1RXS J145434.1+080250: Greater than 3σ from RBSC position. Bade et al. (1998) claim optical−−radio ID is the correct X−ray source. Optical and radio information point towards a correlation.
1RXS J145507.9+192025: High resolution radio position from Laurent-Muehleisen et al. (1997) confirms ID.
1RXS J145715.4+222026: Member of cluster MS 1455.0+2232.
1RXS J145904.1−084254: Better radio resolution needed to confirm ID.
1RXS J150020.7+212213: Member of cluster Abell 2009.
1RXS J151056.3+054431: Member of cluster Abell 2029.
1RXS J151127.2+062153: Greater than 3σ from RBSC position. Optical and radio information point towards a correlation. Member of cluster Abell 2033. Possible X-ray cluster emission?
1RXS J151642.4+070058: Member of cluster Abell 2052.
1RXS J151845.3+061340: High resolution radio position from Laurent-Muehleisen et al. (1997) confirms ID. Member of cluster Abell 2055.
1RXS J152151.0+074221: Member of cluster MKW 03s.
1RXS J152305.7+083550: ID greater than 3σ of RBSC position. There is a strong optical/radio candidate (CGCG 077-097) located within the cluster Abell 2063.
1RXS J153950.3+304305: Member of cluster Abell 2110.
1RXS J154009.4+141116: High resolution radio position from Laurent-Muehleisen et al. (1997) confirms ID (a star?).
1RXS J155611.0+662123: Association with cluster Abell 2146.
1RXS J160435.1+174333: High resolution X-ray position from Burstein et al. (1997) confirms ID.
1RXS J160456.8+235604: Member of cluster AWM 4.
1RXS J160740.7+254106: Optical ID is offset from strong radio source (FIRST ID), possibly indicative of a misidentification with a foreground star.
1RXS J161546.9−060841: Radio emission is very diffuse, from multiple components. Better radio resolution needed. Asso-

ciation.
1RXS J161711.4+063816: No object found within 3σ of X−ray source − X−ray errors too conservative? Identified as RGB J1617+066. Optical and radio information point towards a correlation. High resolution radio position from Laurent-Muehleisen et al. (1997).
1RXS J162032.0+295321: Member of cluster Abell 2175.
1RXS J162100.4+254547: Member of Abell 2177.
1RXS J162837.7+393249: Member of cluster Abell 2199.
1RXS J163246.8+053423: Member of cluster Abell 2204
1RXS J164022.1+464215: Member of cluster Abell 2219
1RXS J164238.9+272621: Member of cluster Abell 2223.
1RXS J170242.5+340336: Member of cluster Abell 2244
1RXS J170941.2+342529: Member of cluster Abell 2249.
1RXS J171519.5+572430: Member of cluster CID 71.
1RXS J171706.8+293117: Member of cluster RBS 1634.
1RXS J171718.9+422652: Member of cluster RX J17173+4227.
1RXS J171746.9+194057: Association with cluster Abell 2254.
1RXS J171810.9+563955: Member of cluster ZwCl 1717.9+5636.
1RXS J172009.3+263727: Member of cluster RX J17201+2637.
1RXS J172226.7+320752: Member of cluster Abell 2261.
1RXS J173257.0+403635: Association with cluster Abell 2272.
1RXS J173301.7+434533: Member of cluster CID 72.
1RXS J174414.3+325925: Member of cluster ZwCl 1742.1+3306.
1RXS J175004.4+470037: High resolution radio position from Laurent-Muehleisen et al. (1997) confirms ID.
1RXS J175441.9+680334: Cluster ZwCl 1754.5+6807 (z = 0.07700) is $53''$ from ID and overlaps within positional errors.
1RXS J175706.9+535130: Member of cluster Abell 2292.
1RXS J182157.4+642051: High resolution radio position from Laurent-Muehleisen et al. (1997) confirms ID.
1RXS J203445.3−354921: Member of cluster Abell 3695.
1RXS J210027.7−170913: Better radio resolution needed to confirm ID.
1RXS J210707.7−252643: Cluster Abell 3744 is nearby and provides a considerable amount of diffuse radio emission as well. Better radio resolution needed.
1RXS J212706.7−120927: Greater than 3σ of RBSC position. Optical and radio information point towards a correlation.
1RXS J213414.4−311737: Better radio resolution needed to confirm ID.
1RXS J213504.7+085807: Optical ID is actually a composite of a bright star and another fainter source.
1RXS J214015.3−233946: Member of cluster MS 2137.3−2353.
1RXS J215336.1+174111: Member of cluster Abell 2390.
1RXS J215541.5+123144: Probable member of cluster Abell 2396
1RXS J221020.8−121040: Probable member of cluster Abell 2420.
1RXS J221614.9−092033: Greater than 3σ of RBSC position. Optical and radio information point towards a correlation. Possible X-ray cluster emission?
1RXS J224919.5−372724: Member of cluster Abell S1065.
1RXS J225019.2+105406: Member of cluster Abell 2495.
1RXS J225334.1−334309: Member of cluster Abell 3934.
1RXS J230714.9−151322: Member of cluster Abell 2533.
1RXS J231607.5−202739: Member of cluster Abell 2566.
1RXS J231712.8+184237: Member of group HCG 094.
1RXS J231829.5+184246: Greater than 3σ of RBSC position. Optical and radio information point towards a correlation. Member of cluster Abell 2572. Possible X-ray cluster emission?
1RXS J232125.9−231230: Probable member of cluster Abell 2580.
1RXS J232519.4−120741: Member of cluster Abell 2597.
1RXS J233631.0+210848: Member of cluster Abell 2626.
1RXS J233641.8+235526: Member of cluster Abell 2627.
1RXS J233827.6+270045: Greater than 3σ of RBSC position. Optical and radio information point towards a correlation. Member of cluster Abell 2634. Pointed *ROSAT* HRI observations by Sakelliou & Merrifield 1998 show X-ray emission is a blend of cluster and individual galaxy emission.
J234741.2−280829: X-ray emission appears to be from bright knot in radio jet. Optical and radio information point towards a correlation.
1RXS J235034.7+292924: Cluster MS 2348.0+2913 (z = 0.09500) is $22''$ from ID and overlaps within positional errors. KPNO spectrum obtained. Strong absorption features at z =-0.00020, possibly a foreground star amid the cluster. Better

optical and radio resolution needed to clarify.
1RXS J234741.2−280829: ID greater than 3σ of RBSC position. There is a strong optical/radio candidate nearby. Member of cluster Abell 4038.

3.2. Previous RBSC Misidentifications?

1RXS J000856.1+411034: Better radio resolution needed. Possible X-ray ID does not seem to be B3 0006+408 (as identified in RGB), but rather a bright, diffuse object at 00h08m56.0s +41d10m09.1s.
1RXS J001144.5+322441: Radio ID is 87GB 000913.4+320913 (as identified in RGB), and X−ray ID is cluster Abell 0007.
1RXS J220220.8+035306: Optical/X−ray ID greater than 3σ from radio position (NVSS and RGB). Background radio object misidentified with B=13.2 X-ray star?

3.3. A simple, well-defined sample of AGN

The RBSC-NVSS sample is defined by the following criteria:

- RBSC count rate ≥ 0.1 counts s^{-1}
- $f_r \geq 2.5 mJy$
- $\delta \geq -40°$
- $|b| \geq 15°$

Columns 1 and 2 of Table 3 summarize the results of the selection process. We should note here, that while the method we employ here is quite robust, the large number of RBSC sources and the loose positional errors dictate that there will be some spurious spatial coincidences. To estimate the number of false matches we might have, we shifted the X-ray positions by $8'$ and performed the identification procedure again. The results are listed in column 3 of Table 3, where we find that the expected percentage of spurious matches is around 3% for reliabilities above 0.50. This fraction could be further reduced by comparing the flux density and magnitude distributions of the true and spurious objects; most spurious sources lie near the NVSS and USNO survey limits, while RBSC-NVSS sources do not.

Forthcoming papers in this series will present the radio, optical, and X-ray properties of the sample and optical identifications and classifications of a subset of objects. Using a number of criteria, we find that this sample of 1512 extragalactic objects is comprised almost entirely of AGN, making this the largest, complete sample of its kind. It represents a major step forward in the identification of RBSC objects and contains a large sample of both radio-loud *and* radio-quiet X-ray objects (previous surveys of this type have typically sampled only the radio-loud population).

FEB thanks W. Brinkmann and J. Siebert for their helpful comments and assistance with the RBSC. He also acknowledges support from a National Radio Astronomy Observatory Jansky Predoctoral Fellowship and a NASA Virginia Space Grant Consortium Fellowship. JJB acknowledges support from the NSF through grant AST 9320547. This research has made use of data obtained through the High Energy Astrophysics Science Archive Research Center Online Service, provided by the NASA/Goddard Space Flight Center, the NASA/IPAC Extragalactic Database (NED) which is operated by the Jet Propulsion Laboratory, Caltech, under contract with the National Aeronautics and Space Administration and the SIMBAD database, operated at CDS, Strasbourg, France. The Digitized Sky Surveys were produced at the Space Telescope Science Institute under US government grant NAG W-2166.

Table 3. RBSC-NVSS Results

Selection criteria imposed	No. of identifications found	No. of spurious identifications expected
RBSC sample	18811	–
Count rate ≥ 0.1 count s^{-1}	8547	–
$\lvert b\rvert \geq 15°$, $\delta \geq -40°$	5441	–
RBSC-NVSS matches with Δ position $< 3\sigma$ and $f_r \geq 2.5$ mJy	2300	919
Linked cross-identification matches	1556	51*

*The flux density and magnitude distributions of the spurious identifications are markedly different from the RBSC-NVSS sample,

REFERENCES

Arimoto, N. , Matsushita, K. , Ishimaru, Y. , Ohashi, T. & Renzini, A. 1997, ApJ, 477, 128

Bahcall, J. N. and Soneira, R. M. 1980, ApJS, 44, 73

Bade, N., Engels, D., Voges, W., Beckmann, V., Boller, Th., Cordis, L., Dahlem, M., Englhauser, J., Molthagen, K., Nass, P., Studt, J. & Reimers, D. 1998, A&A, 127, 145 and `ftp://ftp.hs.uni-hamburg.de/pub/outgoing/rass-id/rass2idv2_0.cat`

Bauer, F. B., Thuan, T. X., & Condon, J. J., in preparation

Brinkmann, W., Siebert, J., Reich, W., Furst, E., Reich, P., Voges, W., Trumper, J., & Wielebinski, R. 1995, A&AS, 109, 147

Brinkmann, W., Laurent-Muehleisen, S., Voges, W., Siebert, J., Becker, R., Brotherton, M., White, R. and Gregg, M., A&A, 2000, in press

Burstein, D. , Jones, C., Forman, W., Marston, A. P. & Marzke, R. O. 1997, ApJS, 111, 163

Ceballos, M. T. & Barcons, X. 1996, MNRAS, 282, 493

Condon, J. J., Anderson, E., & Broderick, J. J. 1995, AJ, 109, 2318

Condon, J. J., Cotton, W. D., Greisen, E. W., Yin, Q. F., Perley, R. A., Taylor, G. B., & Broderick, J. J. 1998, AJ, 115, 1693 and `http://www.cv.nrao.edu/~jcondon/nvss.html`

Condon, J., Kaplan, D. & Yin, Q. 1997, BAAS, 191, 1402

Condon, J. J., Yin, Q. F., Thuan, T. X. & Boller, Th. 1998, AJ, 116, 2682

Dickey, J.M., & Lockman, F.J. 1990, ARA&A, 28, 215

Evans, T. 1988, Ph.D. Thesis, Univ. Cambridge

Fabbiano, G., Kim, D. -W. & Trinchieri, G. 1992, ApJS, 80, 531

Hasinger, G., Truemper, J. & Schmidt, M. 1991, A&A, 246, L2

Lasker, et al. 1990, AJ, 99, 2019

Laurent-Muehleisen, S. A., Kollgaard, R. I., Ryan, P. J., Feigelson, E. D., Brinkmann, W., & Siebert, J. 1997, A&AS, 122, 235

Li, J. & Jin, W. 1996, A&AS, 120, 201

Monet, D., Bird, A., Canzian, B., Harris, H., Reid, N., Rhodes, A., Sell, S., Ables, H., Dahn, C., Guetter, H., Henden, A., Leggett, S., Levison, H., Luginbuhl, C., Martini, J., Monet, A., Pier, J., Riepe, B., Stone, R., Vrba, F., & Walker, R. 1996, USNO-A1.0, (U.S. Naval Observatory, Washington DC) and http://www.usno.navy.mil/pmm/

Moshir, M. et al. 1992, Explanatory Supplement to the IRAS Faint Source Survey, Version 2, JPL D-10015 8/92 (Jet Propulsion Laboratory, Pasadena)

NED 1999, http://nedwww.ipac.caltech.edu/NED.html

Owen, F. N., White, R. A. & Ge, J. 1993, ApJS, 87, 135

Peres, C. B., Fabian, A. C., Edge, A. C., Allen, S. W., Johnstone, R. M. & White, D. A. 1998, MNRAS, 298, 416

Sakelliou, I. & Merrifield, M. R. 1998, MNRAS, 293, 489

Sutherland, W. & Saunders, W. 1992, MNRAS, 259, 413

Voges, W. et al. 1999, A&A, 349, 389

White, R. L., Becker, R. H., Helfand, D. J., & Gregg, M. D. 1997, ApJ, 475, 479 and http://sundog.stsci.edu/

Windhorst, R. A., Kron R. G., & Koo, D. C. 1984, A&AS, 58, 39

This preprint was prepared with the AAS LaTeX macros v5.0.

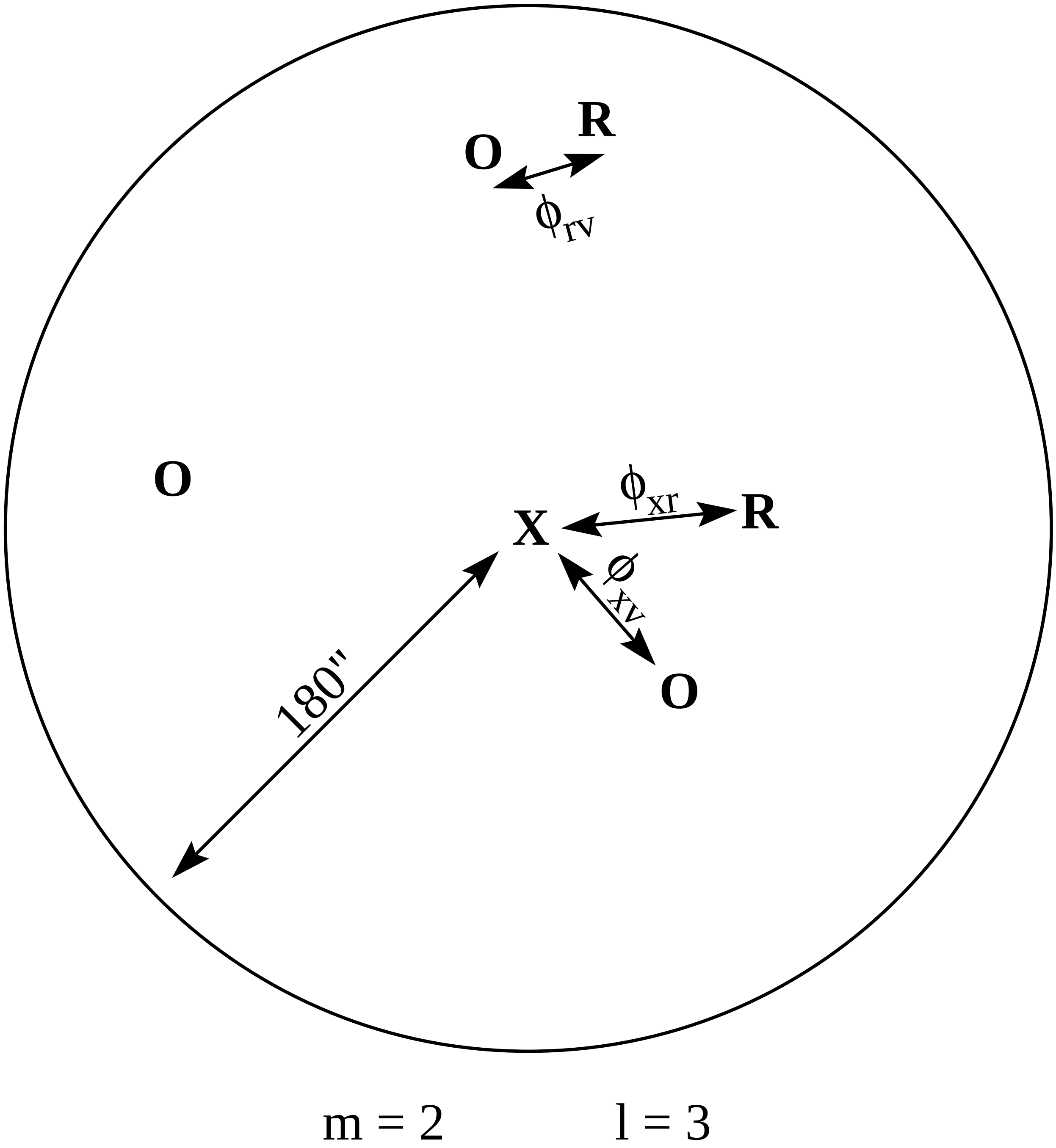

Fig. 1.— Diagram of a typical RBSC-NVSS field. Each search area contains some numbers $m \geq 0$ of NVSS radio sources and $l \geq 0$ of optical objects from the USNO catalog. In this case, there are three optical sources (O) and two radio sources (R) positionally offset from the X-ray source (X) by varying angles (ϕ).

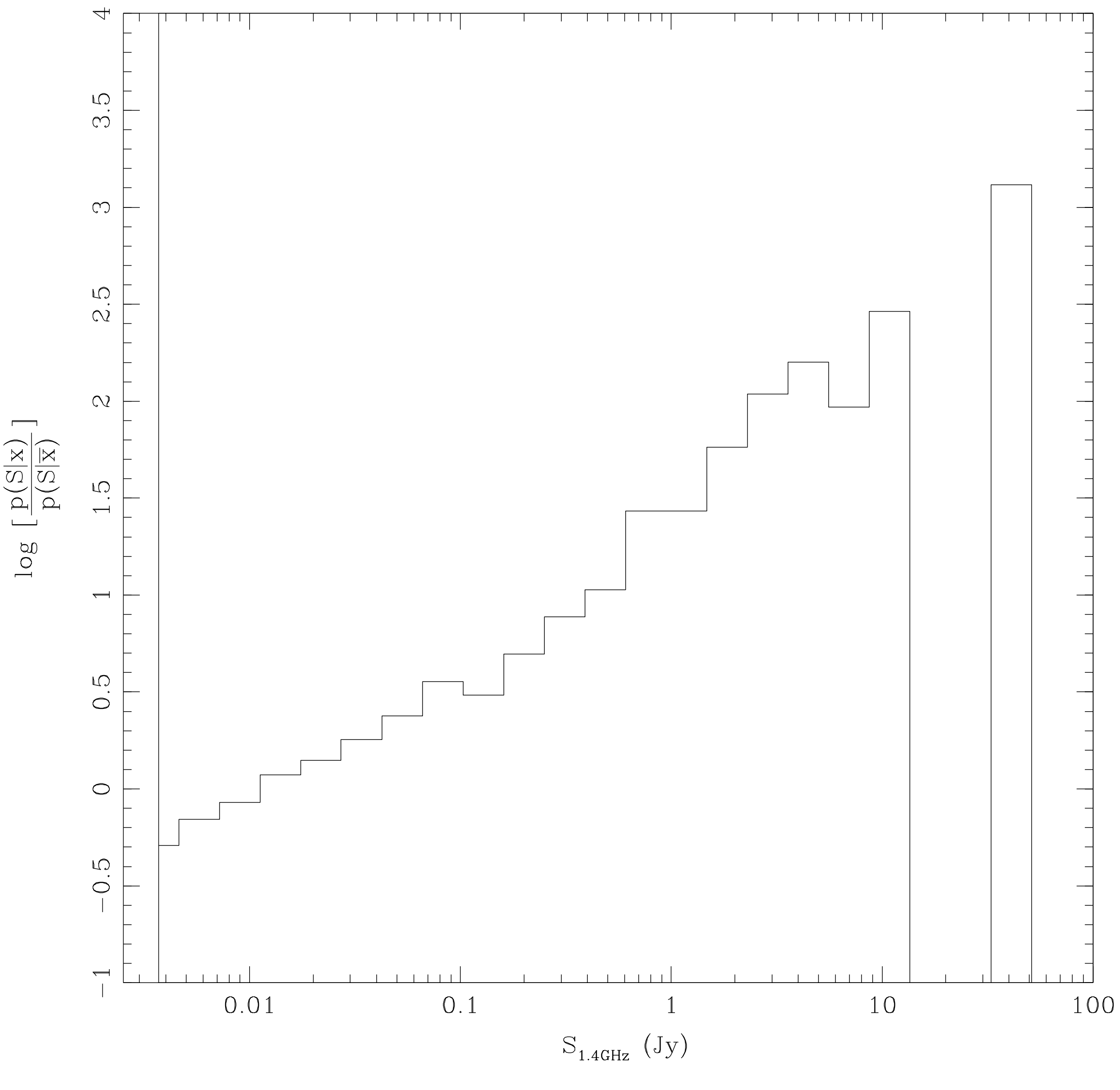

Fig. 2.— Logarithm of the ratio of the probability $p[S|x]$ that a RBSC-NVSS source has flux density S to the probability $p[S|\overline{x}]$ that an unrelated NVSS sources has flux density S. This plot indicates that most background radio sources are much fainter than the true radio identifications of X-ray sources and can be exploited to enhance the probabilities of identifications of strong radio candidates.

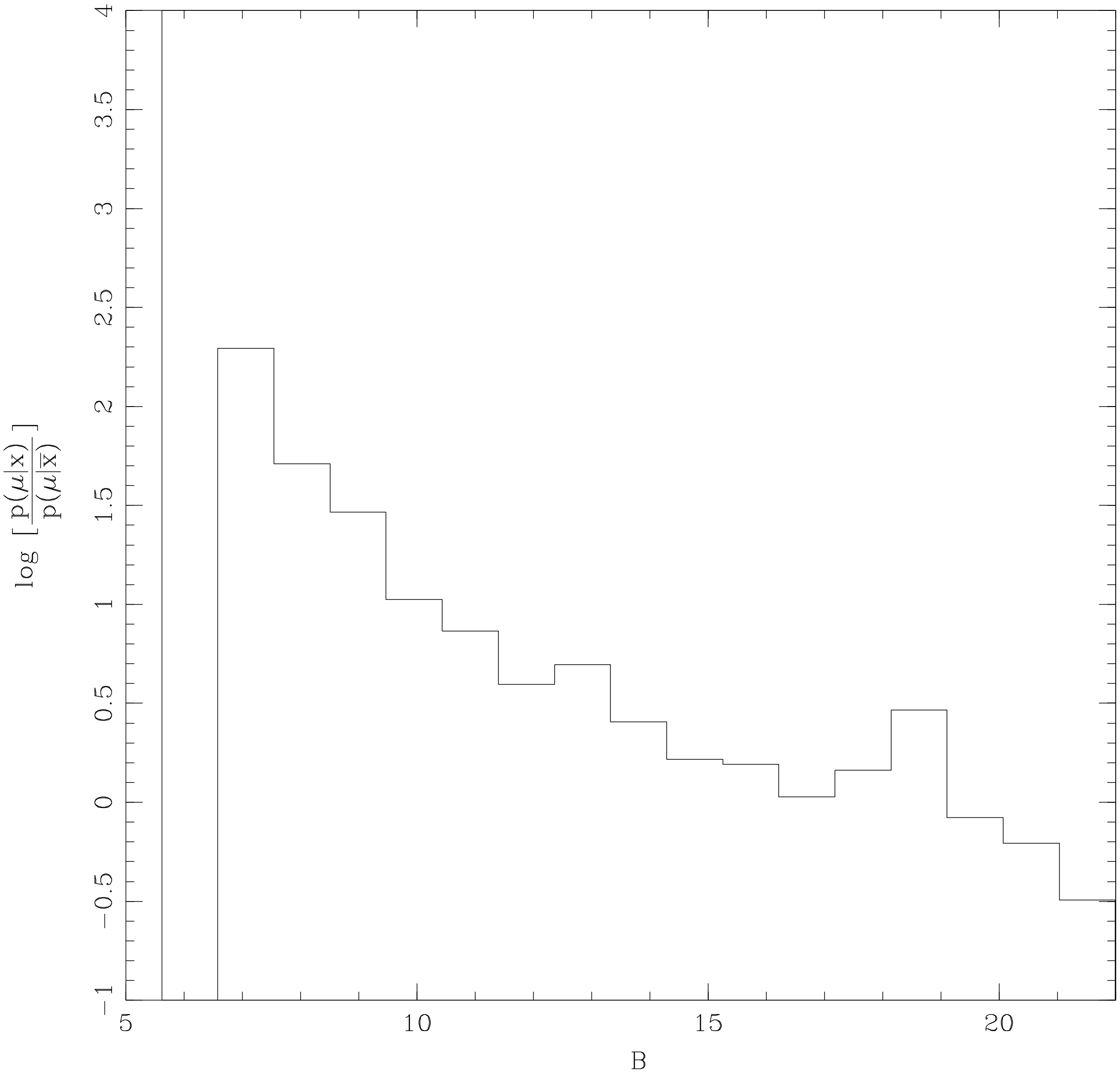

Fig. 3.— Logarithm of the ratio of the probability $p[\mu|x]$ that a RBSC-NVSS optical identification has magnitude μ to the probability $p[\mu|\overline{x}]$ that an unrelated USNO object (Bahcall & Soneira 1980) has magnitude μ. This plot demonstrates that the magnitude distribution of background optical sources is similar to the optical identifications of RBSC sources, yielding little or no enhancement of the probabilities of optical counterparts except at bright (B $<$ 13) magnitudes.

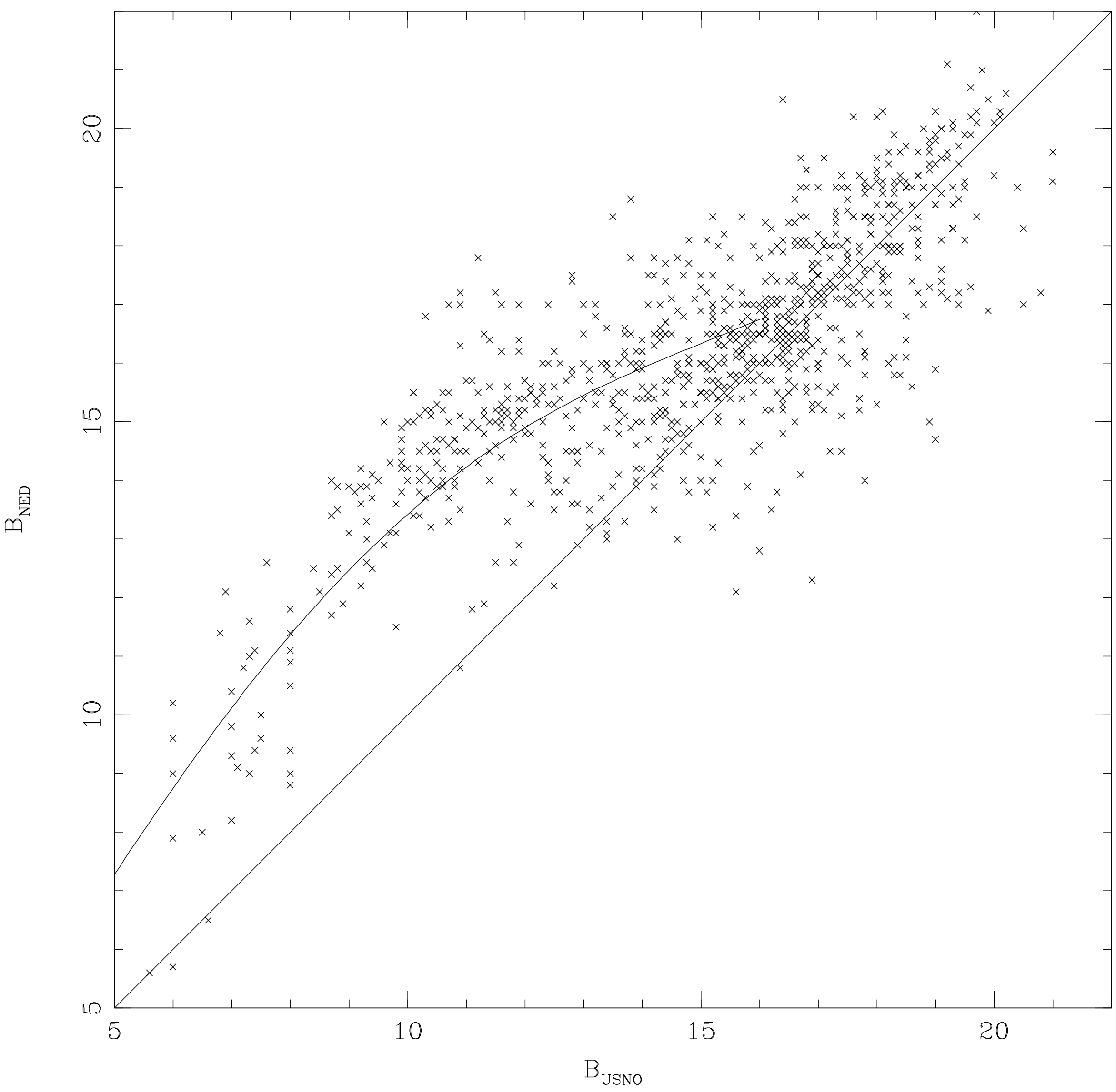

Fig. 4.— Comparison of B_{USNO} and B_{NED}. The straight line represents a one-to-one correspondence and the curve is a least-square fit to the data for $B_{USNO} < 16$ mag.

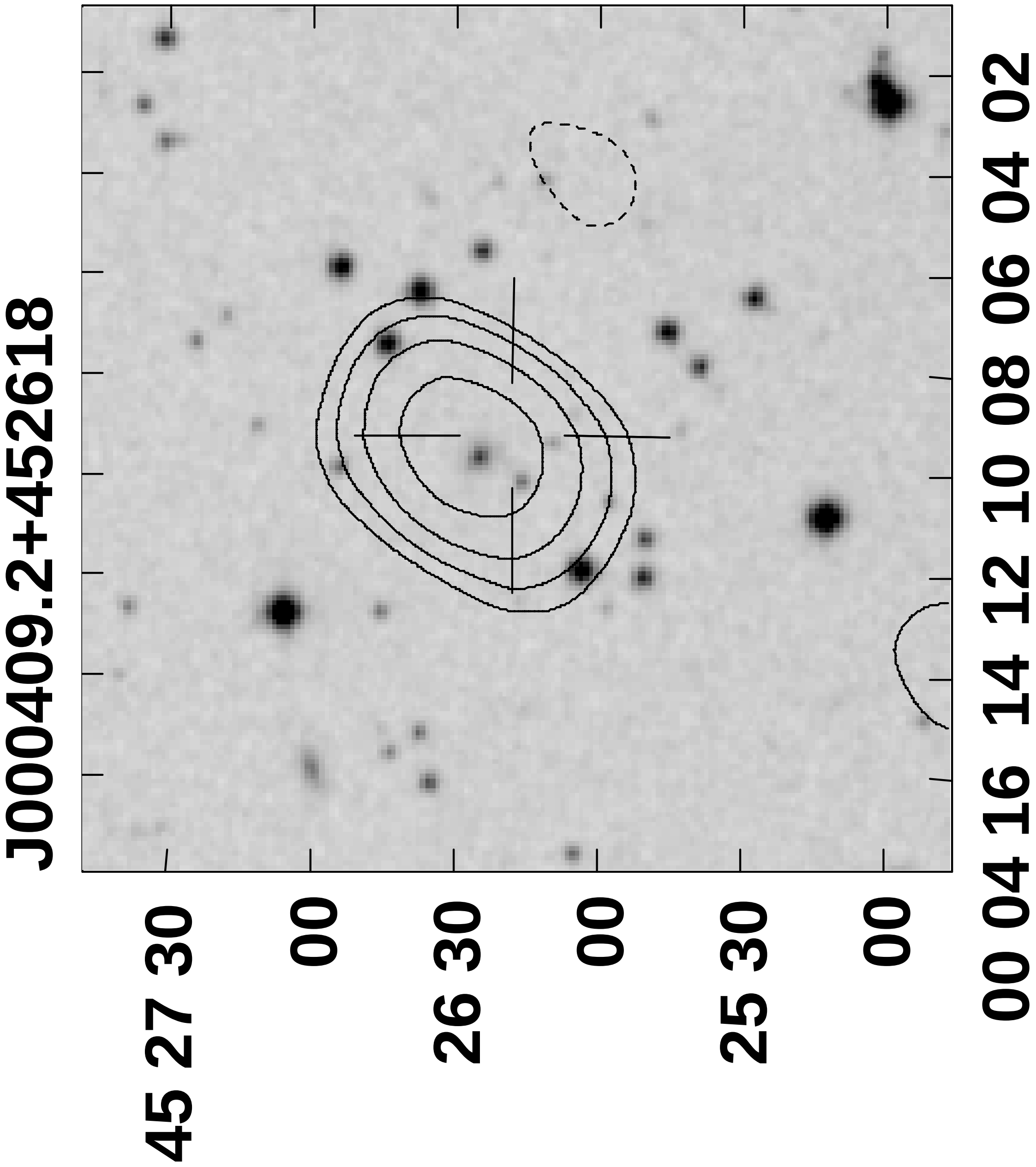

Fig. 5.— Finding charts of RBSC-NVSS sources. The NVSS radio contours are overlaid on the DSS images, and the crosses denote the *ROSAT* error box. In applicable fields, the 3 σ error ellipses of IRAS sources have been plotted.

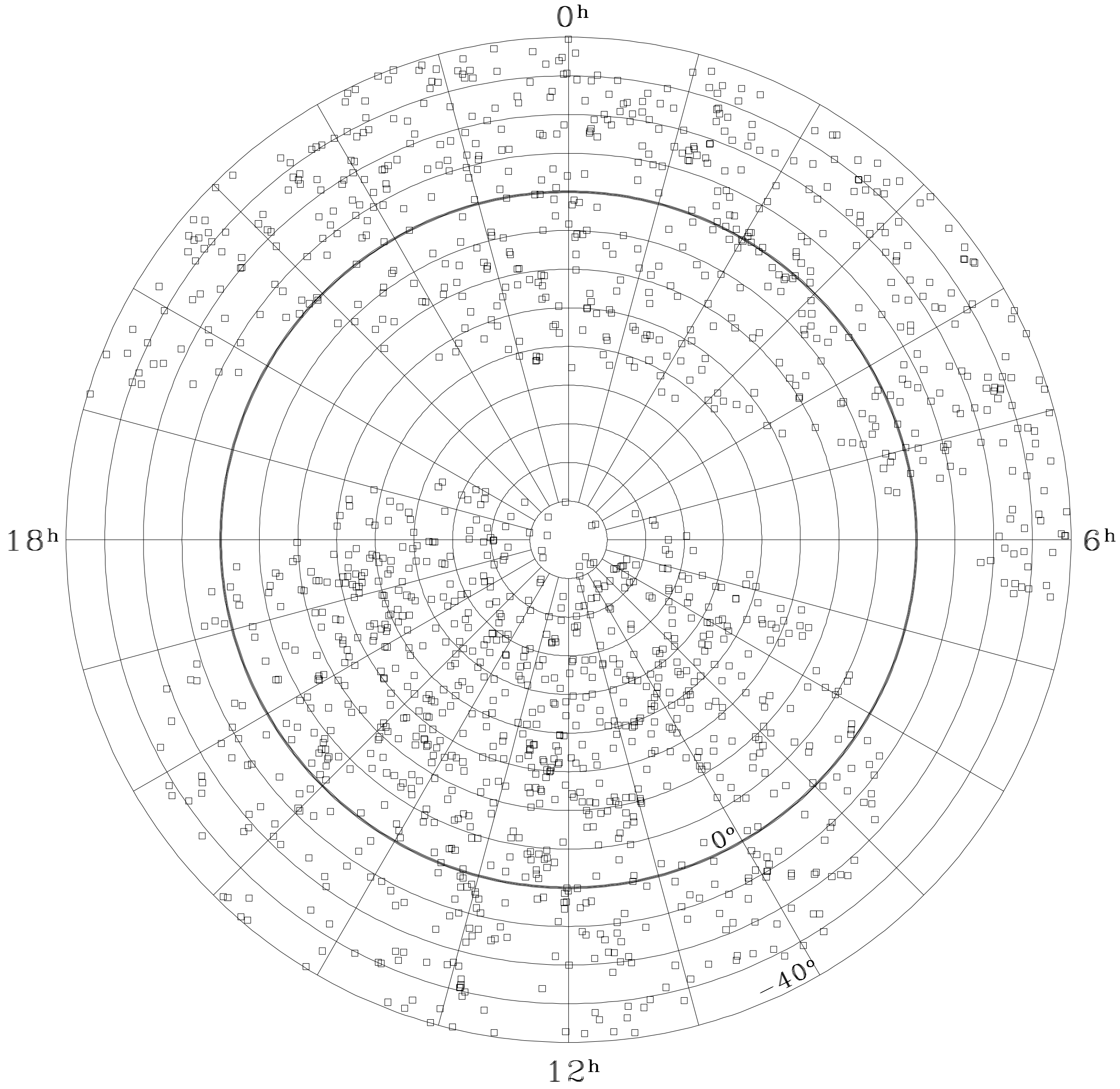

Fig. 6.— The sky distribution of the RBSC-NVSS sources. The overall distribution is fairly uniform in the area $|b| > 15°$, $\delta > -40°$.

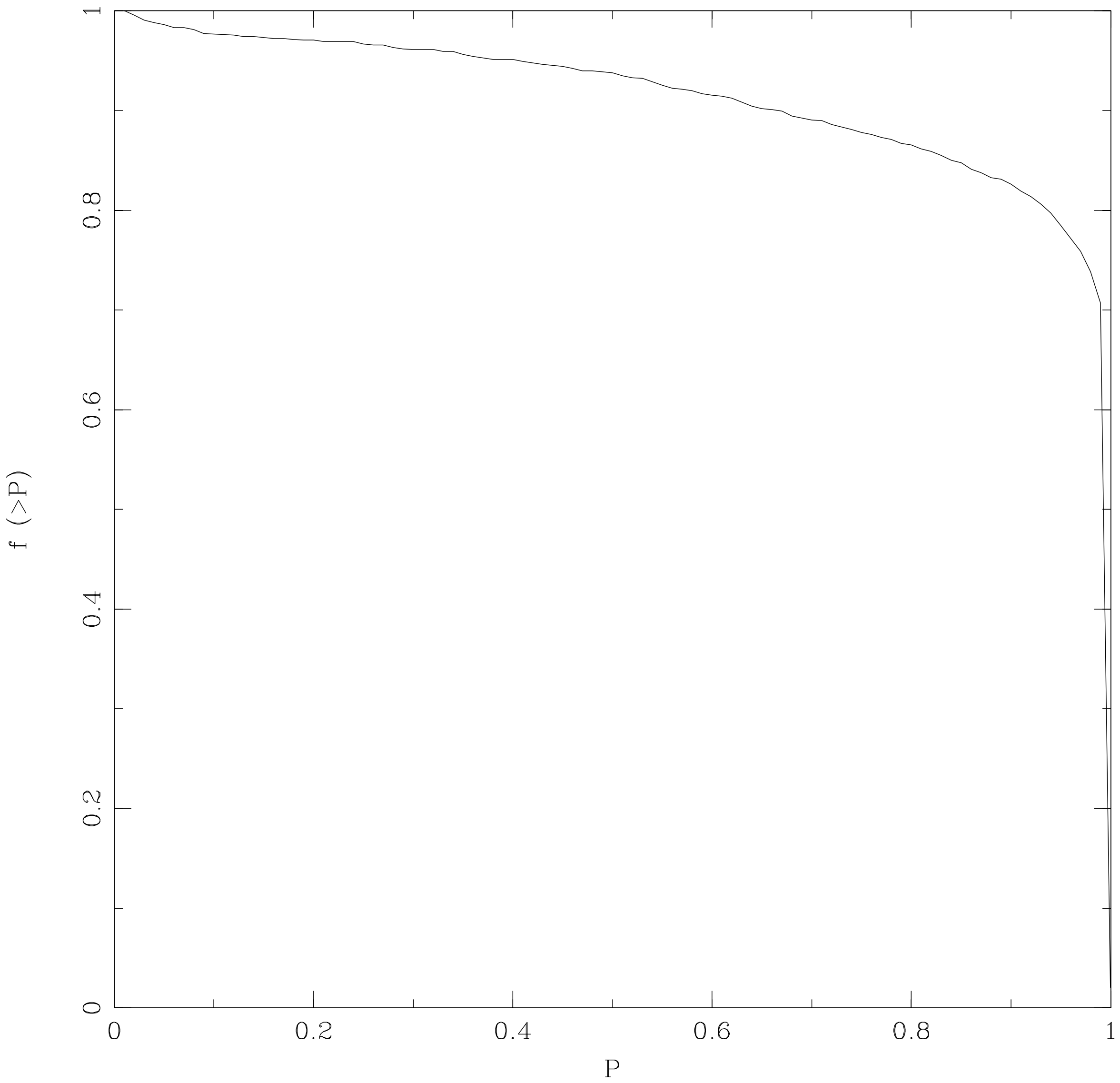

Fig. 7.— The cumulative fraction f of RBSC-NVSS identifications as a function of reliability P (Equation 15).